First Human Imaging Studies with the EXPLORER Total-Body PET Scanner*

Ramsey D. Badawi[1,2], Hongcheng Shi[3], Pengcheng Hu[3], Shuguang Chen[3], Tianyi Xu[4], Patricia M. Price[5], Yu Ding[4], Benjamin A. Spencer[1], Lorenzo Nardo[1], Weiping Liu[4], Jun Bao[4], Terry Jones[1], Hongdi Li[4], and Simon R. Cherry[1,2]

[1]Department of Radiology, University of California Davis Medical Center, Sacramento, California; [2]Department of Biomedical Engineering, University of California, Davis, California; [3]Department of Nuclear Medicine, Zhongshan Hospital Fudan University, Shanghai, China; [4]United Imaging Healthcare, Shanghai, China; and [5]Department of Surgery and Cancer, Imperial College, London, United Kingdom

Within the EXPLORER Consortium, the construction of the world's first total-body PET/CT scanner has recently been completed. The 194-cm axial field of view of the EXPLORER PET/CT scanner is sufficient to cover, for the first time, the entire human adult body in a single acquisition in more than 99% of the population and allows total-body pharmacokinetic studies with frame durations as short as 1 s. The large increase in sensitivity arising from total-body coverage as well as increased solid angle for detection at any point within the body allows whole-body ^{18}F-FDG PET studies to be acquired with unprecedented count density, improving the signal-to-noise ratio of the resulting images. Alternatively, the sensitivity gain can be used to acquire diagnostic PET images with very small amounts of activity in the field of view (25 MBq, 0.7 mCi or less), with very short acquisition times (~1 min or less) or at later time points after the tracer's administration. We report here on the first human imaging studies on the EXPLORER scanner using a range of different protocols that provide initial evidence in support of these claims. These case studies provide the foundation for future carefully controlled trials to quantitatively evaluate the improvements possible through total-body PET imaging.

Key Words: instrumentation; PET; EXPLORER; FDG; PET/CT; total-body PET

signal collection efficiency can be realized through extending the axial extent of the scanner, with the highest collection efficiency being approached as the scanner becomes long enough to cover the entire human body. A further key motivating factor for increasing the axial extent so dramatically is that it becomes possible to perform total-body dynamic studies, where tracer kinetic modeling with an image-derived input function to estimate model microparameters can be performed across all the organs and tissues of the body with high temporal resolution. Thus, the idea of developing long-axial-field-of-view (FOV) scanners, and ultimately total-body scanners, has been studied over many years and has recently gained increasing traction (1,2).

In 2005, our team at UC Davis committed to developing a PET scanner long enough to simultaneously image the entire human body. Monte Carlo simulations suggested that the total-body imaging geometry could provide gains of up to 40-fold in effective count rate for total-body applications compared with a more conventional 22-cm-axial FOV scanner, if time-of-flight (TOF) effects are included (3,4). Gains of a factor of approximately 4-fold were predicted for single-organ imaging. These gains could be used either to (1) deliver enhanced image quality, (2) reduce scan time, (3) increase the time window after injection when scanning is possible, (4) reduce dose, or some combination of these.

C urrent-generation clinical PET/CT and PET/MR scanners typically cover an axial extent of 15–30 cm. Large increases in
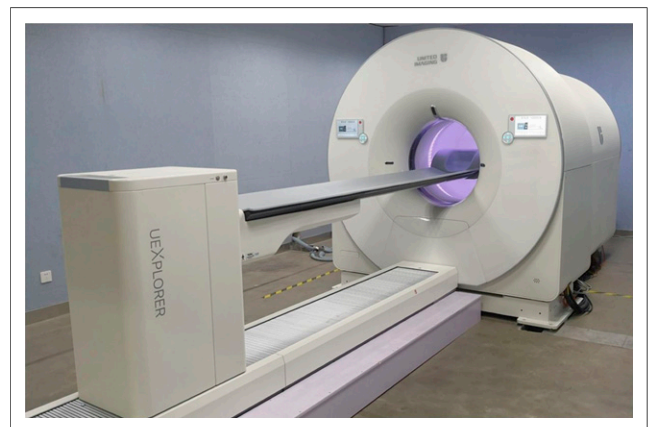
FIGURE 1. Photograph of completed EXPLORER total-body PET/CT scanner.

TABLE 1
Subject Demographics and Injected Activity

Subject	Sex	Age (y)	Weight (kg)	Height (cm)	Blood glucose level (mmol/L)	Injected activity (MBq)
1	Male	61	65	163.5	4.9	290 (7.8)
2	Female	61	56	156.0	4.8	256 (6.9)
3	Female	63	55	150.0	4.3	81 (2.2)
4	Female	45	43.5	152.0	5.1	25 (0.68)

Data in parentheses are mCi.

In 2011, initial funding was obtained through the National Cancer Institute's (NCI) provocative questions award, which facilitated the formation of the EXPLORER Consortium. This Consortium included teams from the University of Pennsylvania and Lawrence Berkeley National Laboratory as well as representatives from industry and several prominent imaging physician-scientists to guide planning. Subsequently, in 2015 we were awarded a National Institutes of Health (NIH) Transformative R01 grant, enabling us to partner with industry and begin construction. The EXPLORER Consortium is now working on 2 devices, one with excellent timing resolution and a final projected length of 140 cm being developed by the University of Pennsylvania team in collaboration with KAGE Medical and Philips (5,6), and the other with excellent spatial resolution and a length of 194 cm being developed by the UC Davis team and United Imaging Healthcare (7). This second device is now complete, and is the first medical scanner of any kind that can acquire simultaneous static and dynamic 3-dimensional images of the entire human body. Here, we report the first total-body images acquired with human subjects on this scanner, which are intended to demonstrate initial feasibility for each of the opportunities we had previously proposed, namely, improved image quality, fast scanning, delayed scanning after many half-lives, low-dose scanning, and total-body pharmacokinetic imaging.

EXPLORER SCANNER

The EXPLORER total-body PET/CT scanner (Fig. 1) has an axial field of view of 194 cm and a transaxial field of view of 68.6 cm. It is integrated with an 80-row, 160-slice CT scanner. The PET detector crystals are made from lutetium (yttrium) oxyorthosilicate and measure 2.76×2.76 mm^2 in cross-section by 18.1 mm in depth. Crystals are arranged in 7×6 arrays with a crystal pitch of 2.85 mm. Each array is read out using 4 6 $\times$ 6 mm^2 silicon photomultipliers. Additional information on the design and performance of the detector and electronics components may be found in Lyu et al. (8). The system is constructed as 8 axial units, each with an axial field of view of 24 cm and with a gap of just 2.5 mm between units. The diameter of the detector ring is 78.6 cm, with a patient bore of 76 cm for the PET portion of the scanner. The system has TOF capability (timing resolution, ~430 psecs) and an energy resolution of 11.7%, and the reconstructed spatial resolution at 1 cm from the center of the field of view, using the NEMA NU-2 2018 protocol (9) and filtered backprojection reconstruction, is approximately 2.9 mm. A full physical and technical evaluation of the scanner will be forthcoming. All images shown in this article are collected using a 430 to 645 keV energy window, accepting coincidences from detector pairs with unit differences up to ± 4 (corresponding to an axial acceptance angle of $\sim \pm 57°$). The coincidence time window varies with unit difference to account for the different pathlengths through the body and ranges from 4.5 to 6.9 ns. Reconstruction was performed using a list-mode ordered-subsets expectation maximization algorithm incorporating TOF and point-spread function modeling (OSEM-TOF-PSF).

HUMAN SUBJECTS

Normal volunteer studies were performed in collaboration with Zhongshan Hospital, Shanghai. The study protocol was approved by the Zhongshan Hospital Ethics Committee, and informed consent was obtained from all subjects. Exclusion criteria included age, younger than 18 y; exercise in the prior 24 h; history of cancer, diabetes, or bladder problems; inability to lie supine and still inside the scanner for the scan duration; inability to give informed consent; and any employee of United Imaging Healthcare. All subjects fasted for at least 6 h before injection with ^{18}F-FDG and scanning. Injections were either into an arm vein or into a vein near the ankle. Demographics and injected activity are shown in Table 1. To explore the dynamic range of the scanner, subjects were injected with a range of doses of ^{18}F-FDG, and scans were acquired at a range of time intervals after injection. Subjects 1 and 2 were injected with standard activities based on weight (4.5 MBq/kg), whereas for subjects 3 and 4 the injected activity was reduced to approximately 30% and approximately 10% of the standard activity, respectively. Motion was minimized, and repositioning was facilitated (where necessary) by use of evacuable positioning bags (model no. R7513-68NL; Klarity Medical Products, Inc.).

NOTEWORTHY

- First human studies on the EXPLORER total-body PET scanner have been performed.
- EXPLORER is the first medical imaging scanner of any kind capable of capturing 3-dimensional images of the entire human body at the same time.
- This is the first study to show the kinetics of an injected radiotracer throughout the entire body.
- Diagnostic-quality scans using acquisition times of approximately 1 min or less can be obtained.
- Injected doses of 25 MBq (0.7 mCi) can be used to acquire diagnostic-quality images.
- EXPLORER has the ability to image ^{18}F-FDG distribution for up to 10 h (<5 half-lives) after injection.
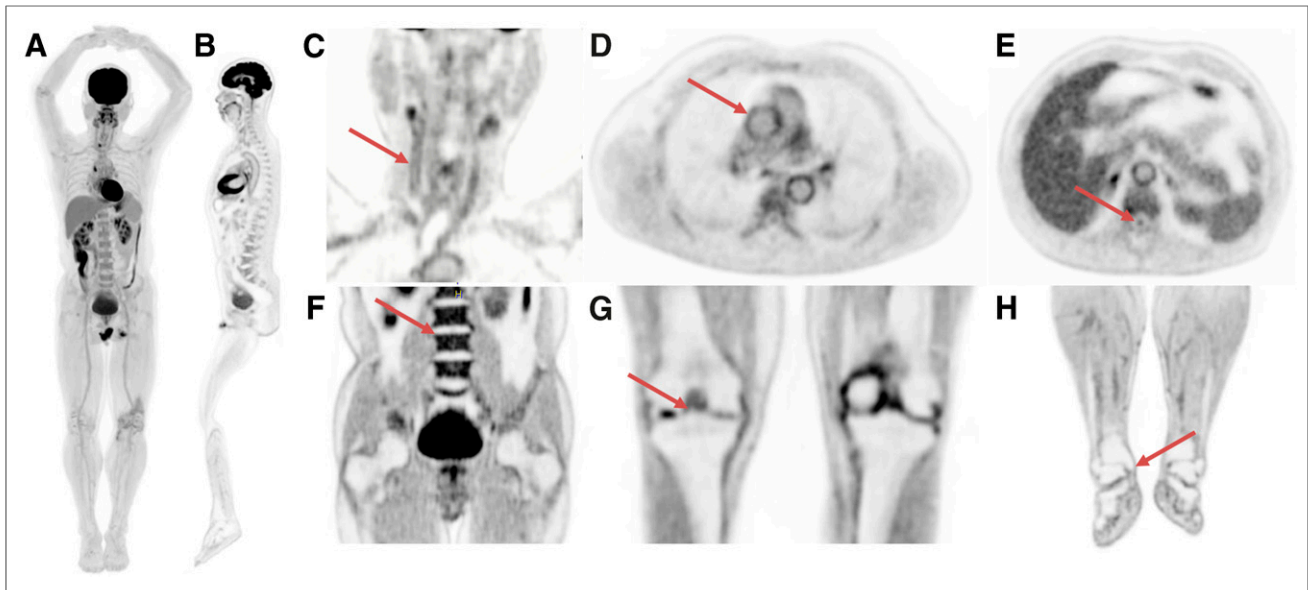
FIGURE 2. Selected views from total-body scan of subject 1. (A) Total-body MIP. (B) Total-body sagittal view. (C) Head/neck view, with arrow indicating walls of right carotid artery. (D) Chest view, showing walls of major blood vessels, with ascending aorta indicated by arrow. (E) Midthoracic view with spinal canal indicated by arrow. (F) Abdomen and pelvis, showing clear delineation of endplates of vertebral bodies (arrow points to superior endplate of L3). (G) Knees, with bone spur indicated by arrow. (H) Lower extremities, with arrow showing delineation of medial tibial malleolus.

Low-dose CT scans were acquired for attenuation correction and all corrections applied to the reconstructed images (randoms correction using delayed coincidence window, scatter correction, deadtime correction, and detector normalization). All data were reconstructed using list-mode OSEM-PSF-TOF, with specific parameters given in the relevant sections below.

HIGH-QUALITY IMAGING

Subject 1 was injected with 290 MBq of ^{18}F-FDG. At 82 min after injection, a 20-min list-mode scan was initiated on the EXPLORER scanner. Data were reconstructed with 20 subsets and 5 iterations on a $1.0 \times 1.0 \times 1.45$ mm^3 voxel grid.

Figure 2 shows a maximum-intensity projection (MIP) and a sagittal slice through the image volume generated from the 20-min scan. Of particular note is the uniformity of the uptake in the liver in the MIP image. Also shown are selected slices focusing on a range of anatomic features. It can be seen that the high count-density afforded by this scanner allows visualization of a range of small features without the drawback of high image noise.

REDUCED SCAN TIME

Total-body data from subject 1 was organized into list-mode datasets of duration 20 min, 10 min, 5 min, 2.5 min, 75 s, 37.5 s, and 18.75 s. The datasets were reconstructed with OSEM-PSF-TOF with 20 subsets and 2 iterations, on a voxel grid of $4.0 \times 4.0 \times 2.85$ mm^3. Representative slices from selected parts of the reconstructed volumes of these sequentially reduced datasets are shown in Figure 3. Unsurprisingly, the apparent noise increases as scan time is decreased, but the images appear to be of diagnostic quality at 37.5 s and are arguably diagnostic even at 18.75 s.

DELAYED IMAGING

Subject 2 underwent total-body PET scanning at 1, 3, 8, and 10 h after injection. At each of the 4 time points, the scan duration was 14 min. The subject ate a planned low-carbohydrate meal after the 3-h scan. The datasets were reconstructed with OSEM-PSF-TOF with 20 subsets and 2 iterations, on a voxel grid of $4.0 \times 4.0 \times 2.85$ mm^3. Figure 4 shows MIPs and sagittal views from the repeated scans. Areas of focal intensity in the lower limb are from contamination. It can be seen that there is significantly more blood clearance at the 3-h time point compared
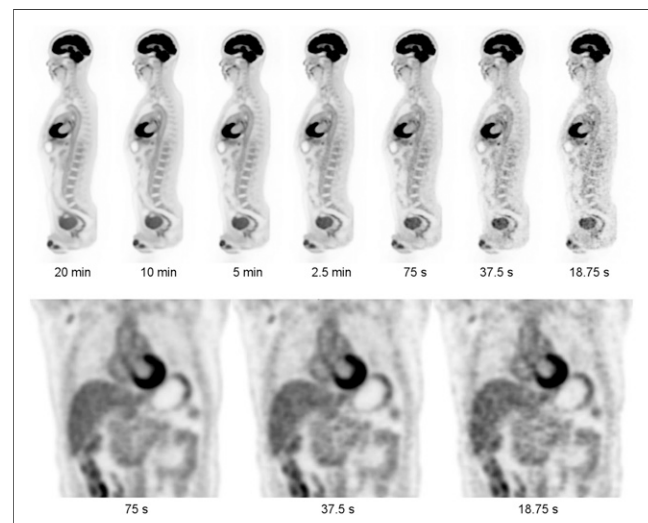

FIGURE 3. Views from subject 1 as function of scan duration (290 MBq injected, 82 min uptake period). (Top) Sagittal views from 20 min to 18.75 s. (Bottom) Coronal views at 75, 37.5, and 18.75 s.
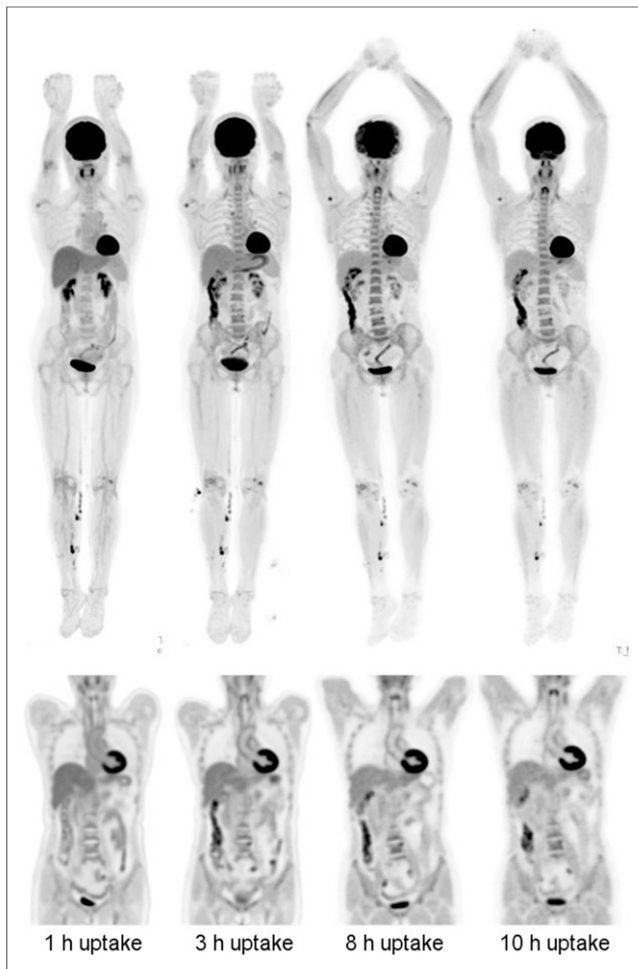
FIGURE 4. Delayed imaging for subject 2 (256 MBq injected, 14 min scan duration). (Left-to-right) Images from scans performed at 1, 3, 8, and 10 h after injection. (Top row) MIP images. (Bottom row) Coronal views of thorax and abdomen. Head motion artifacts are visible in 8-h scan.

FIGURE 5. Low-dose images from subject 4. Subject was injected with 25 MBq and scanned for 10 min after 52.5 min of uptake time. Total-body MIPs (left) and coronal view of upper body (right). Tracer was injected into a vein in right lower leg.

with the 1-h time point. At 10 h after injection, the injected activity had decayed to 5.7 MBq; due to urinary excretion, less than this remained in the field of view. Even at this low amount of activity, the images appear to be of diagnostic quality. Of note, if 8.3 MBq were injected then, ignoring excretion, there would be 5.7 MBq in the field of view after 1 h of uptake (similar to the activity in the subject at the 10-h time point); this would correspond to an effective dose of approximately 0.16 mSv (10).

LOW-DOSE IMAGING

Subject 4 was injected with 25 MBq of activity and scanned for 10 min at 50 min after injection. The datasets were reconstructed with OSEM-PSF-TOF with 20 subsets and 2 iterations, on a voxel grid of $3.125 \times 3.125 \times 2.85$ mm^3. Figure 5 shows an MIP and a coronal view. The images again appear to be of good quality. It should be noted that this subject was particularly small (43.5 kg; 152 cm).

SINGLE-ORGAN IMAGING

Subject 3 was injected with 80 MBq of activity and scanned for 25 min starting at 25 min after injection. The top of the subject's
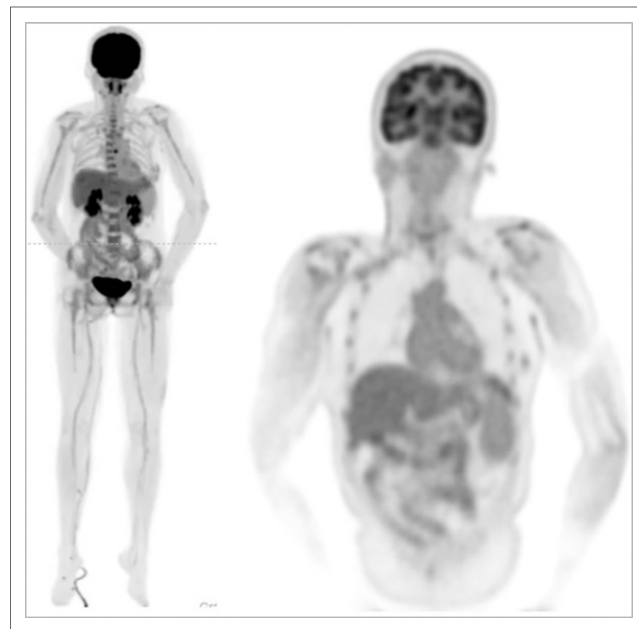
head was positioned approximately 30 cm away from the distal end of the axial field of view of the scanner. Brain images were reconstructed with OSEM-PSF-TOF with 20 subsets and 10 iterations, on a voxel grid of $1.2 \times 1.2 \times 1.45$ mm^3.

Figure 6 shows orthogonal slices through the brain image volume for subject 3. There is excellent delineation of the smaller structures of the brain, with the high sensitivity of the scanner supporting a very-high-resolution reconstruction without incurring a high noise penalty, even at this low injected dose.

TOTAL-BODY DYNAMIC IMAGING

Before the repeated scans obtained for subject 2, data were acquired in list-mode as the subject was injected and subsequently for the next hour. Initial data were binned into frames of 1 s in duration and reconstructed. Figure 7 shows selected frames from this scan, presented from frames within the rotating MIPs. The transit of the bolus from the heart, to the lungs, back to the heart and into the arterial tree can clearly be seen. Figure 7 also shows time–activity curves generated from these images. Of particular note, the high temporal resolution of the scan series allows

FIGURE 6. Dedicated brain scan from subject 3. Motion correction has not been implemented at this time.
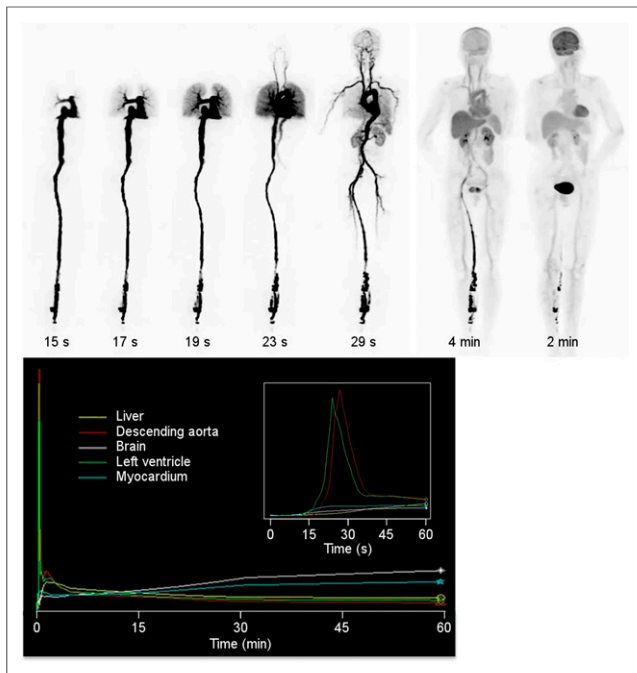
FIGURE 7. Total-body dynamic imaging. (Top) Selections of rotating MIPs from dynamic scan of subject 2. Frame duration is 1 s, except for the 2 left-most images, which have frame durations of 1 min. (Bottom) Time–activity curves for selected anatomic regions. (Bottom inset) Time–activity curves for first minute of acquisition.

measurement of the dispersion between the left ventricle and the descending aorta (inset).

CONCLUSION

The potential benefits of and future applications for total-body PET rest on 5 primary claims, namely that a total-body PET scanner can image better, faster, later after injection, or with lower dose; and that such a device can generate total-body dynamic images with high temporal resolution (*1,2*). Our initial data provide qualitative support for all these claims. Future studies will aim to provide quantitative assessments of these claims, to develop evidence for clinical utility, and to use this new and ground-breaking tool to answer questions in medicine and biology that hitherto could not be answered.

REFERENCES

1. Cherry SR, Badawi RD, Karp JS, Moses WW, Price P, Jones T. Total-body imaging: transforming the role of positron emission tomography. *Sci Transl Med.* 2017;9:eaaf6169.
2. Cherry SR, Jones T, Karp JS, Qi J, Moses WW, Badawi RD. Total-body PET: maximizing sensitivity to create new opportunities for clinical research and patient care. *J Nucl Med.* 2018;59:3–12.
3. Poon JK, Dahlbom ML, Moses WW, et al. Optimal whole-body PET scanner configurations for different volumes of LSO scintillator: a simulation study. *Phys Med Biol.* 2012;57:4077–4094.
4. Badawi RD, Poon JK, Surti S, et al. EXPLORER, an ultrasensitive total-body PET scanner: application feasibility simulations. Paper presented at: the World Molecular Imaging Congress, Savannah, Georgia, September 2013.
5. Viswanath V, Daube-Witherspoon ME, Schmall JP, et al. Development of PET for total-body imaging. *Acta Phys Pol B.* 2017;48:1555–1566.
6. Karp J, Schmall J, Geagan M, et al. Imaging performance of the PennPET Explorer scanner. *J Nucl Med.* 2018;59(suppl 1):222.
7. Badawi R, Liu W, Berg E, et al. Progress on the EXPLORER project: towards a total body PET scanner for human imaging. *J Nucl Med.* 2018;59(suppl 1):223.
8. Lyu Y, Lv X, Liu W, et al. Mini EXPLORER II: a prototype high-sensitivity PET/CT scanner for companion animal whole body and human brain scanning. *Phys Med Biol.* January 8, 2019 [Epub ahead of print].
9. *Performance Measurements of Positron Emission Tomographs (PETs).* NEMA Standards Publication NU 2-2018. Roslyn, VA: National Electrical Manufacturers Association; 2018.
10. Brix G, Lechel U, Glatting G, et al. Radiation exposure of patients undergoing whole-body dual-modality ^{18}F-FDG PET/CT examinations. *J Nucl Med.* 2005;46:608–613.